ROM SAF Report 49
Ref: SAF/ROM/METO/REP/RSR/049
Web: https://rom-saf.eumetsat.int
Date: 14 April 2026

EUMETSAT
ROM SAF
RADIO OCCULTATION METEOROLOGY

ROM SAF Report 49

An initial assessment of the quality of radio occultation data from EPS-SG-A1

Liam J. Hall

Met Office

DOCUMENT AUTHOR TABLE

	Author(s)	Function	Date
Prepared by:	L.J. Hall	ROM SAF Scientist	02 March 2026
Reviewed by:	N.E. Bowler	ROM SAF Local Manager	12 March 2026
Reviewed by:	M. Forsythe	ROM SAF SG Member	19 March 2026
Reviewed by:	S. Healy	ROM SAF Science Co-ordinator	27 March 2026
Approved by:	K.B. Lauritsen	ROM SAF Project Manager	14 April 2026

DOCUMENT CHANGE RECORD

Version	Date	By	Description
1.0	14 April 2026	Liam J. Hall	Final version following internal reviews

ROM SAF

The Radio Occultation Meteorology Satellite Application Facility (ROM SAF) is a decentralised processing centre under EUMETSAT which is responsible for operational processing of radio occultation (RO) data from the Metop, Metop-SG and Sentinel-6 satellites and radio occultation data from other missions. The ROM SAF delivers bending angle, refractivity, temperature, pressure, humidity, and other geophysical variables in near real-time for NWP users, as well as reprocessed Climate Data Records (CDRs) and Interim Climate Data Records (ICDRs) for users requiring a higher degree of homogeneity of the RO data sets. The CDRs and ICDRs are further processed into globally gridded monthly-mean data for use in climate monitoring and climate science applications.

The ROM SAF also maintains the Radio Occultation Processing Package (ROPP) which contains software modules that aid users wishing to process, quality-control and assimilate radio occultation data from any radio occultation mission into NWP and other models.

The ROM SAF Leading Entity is the Danish Meteorological Institute (DMI), with Cooperating Entities: i) European Centre for Medium-Range Weather Forecasts (ECMWF) in Reading, United Kingdom, ii) Institut D'Estudis Espacials de Catalunya (IEEC) in Barcelona, Spain, iii) Met Office in Exeter, United Kingdom, and iv) and Wegener Center, University of Graz, in Graz, Austria. To get access to our products or to read more about the ROM SAF please go to: https://rom-saf.eumetsat.int.

Intellectual Property Rights

Abstract

EUMETSAT's Polar System Second Generation Satellite A1 (EPS-SG-A1, hereafter referred to as Metop-D), was successfully launched on 13th August 2025. Along with the European Union's Copernicus Sentinel-5 spectrometer which is hosted on EPS-SG-A1, Metop-D provides critical data for numerical weather prediction (NWP), weather and climate monitoring as part of the EU's Joint Polar System (EPS). Dissemination of radio occultation L1 bending angle data via EUMETCast first started on 6th November 2025, and The Met Office first received data on 17th November 2025, and these data have been monitored since.

Metop-D provides around 1,200 occultations per day, around double the volume from Metop-B and Metop-C separately. L1 bending angle data from Metop-D were compared with those from Metop-B, Metop-C, PlanetiQ and Spire. Notably, Metop-D shows improved $O-B$ standard deviations particularly at higher and lower levels relative to all comparison satellites. Bending angle $O-B$ biases are broadly similar to those of Metop-B, Metop-C, PlanetiQ and Spire in the core region, with slightly larger biases at higher levels (more positive) compared to all the other satellites and in the lower troposphere (more negative) compared to PlanetiQ and Spire. Met Office statistics also show a more positive mean bias in the upper stratosphere, while ECMWF statistics show a negative bias in the same region; this behaviour is consistent across all other satellites.

An NWP experiment assimilating Metop-D data was conducted over a three-month period and verified using the root mean square error, or RMSE. The addition of observations from Metop-D improves the forecast skill, with a mean impact of 0.19% and 0.20%, against observations and ECMWF analyses. The addition of these $\sim$1,200 profiles per day ($\sim$1,100 after quality control) shows improvements in all regions across different variables with minimal degradation. The inclusion of Metop-D clearly decreases the standard-deviation ratios for the radio occultation observation type. There is little reduction in the standard-deviation ratios for other observation types.

The timeliness of Metop-D L1 data has not improved relative to Metop-B and Metop-C, averaging 52 and 25 minutes longer to receive data, respectively. This is understood to be due to the data transfer method that the Met Office uses while Metop-D is pre-operational. In comparison to FY-3E, Metop-D is much quicker, having received data 2 hours and 20 minutes sooner than FY-3E for the same time period. This allows the majority of observations to be included within the assimilation window. Timeliness is expected to improve once EUMETSAT makes Metop-D operational. Operational assimilation of bending angles from Metop-D by the Met Office is expected around June 2026.

Contents

1 Introduction

EUMETSAT had previously launched three satellites for their polar system, EPS, to provide crucial data for weather forecasting and climate monitoring. These were Metop-A, Metop-B and Metop-C. Since then, Metop-A was decommissioned after nearly 15 years of service, leaving behind Metop-B and Metop-C. As part of EUMETSAT's continued commitment to providing high-quality data, EUMETSAT launched the first of six new second-generation polar-orbiting satellites, Metop-D, on 13th August 2025.

Launched in a 09:30 descending, sun-synchronous orbit at an altitude of 835 km, Metop-D carries a suite of instruments including a radio occultation (RO) sounder, which measures the phase delay during an occultation between the satellite and navigational satellites (Global Navigation Satellite System – GNSS). This is crucial for data assimilation in Numerical Weather Prediction (NWP) models. The new RO sounder on the second-generation satellites has been designed to improve on the previous RO instrument, GRAS (GNSS Receiver for Atmospheric Sounding). It is capable of handling three times more occultations than GRAS, whilst improving vertical coverage for space weather applications (ESA, 2026).

Monitoring of L1 bending angle data is ongoing, with comparisons against relevant satellites. Experiments ran between 17th November 2025 and 17th February 2026, during which the forecasts were evaluated against observations and ECMWF analyses. L2 refractivity data are expected to be disseminated towards the end of March and early April 2026; therefore, an assessment of L2 data cannot be performed at present.

2 Bending angle evaluation

Metop-D has been providing L1 bending angle (BA) data to EUMETCast since 6th November 2025, and the Met Office first received this data on 17th November 2025. Bending angles were evaluated against Met Office background data whilst also comparing mean bias and standard deviation with Metop-B, Metop-C, PlanetiQ and Spire, all of which are processed by EUMETSAT.

As Metop-D uses an improved RO instrument that tracks a wider set of GNSS constellations than the GRAS instruments on Metop-B and Metop-C, it provides around 1,200 occultations per day, roughly twice as many as Metop-B and as Metop-C. After passing quality control, around 1,100 are accepted at the Met Office.

2.1 Mean bias and standard deviation

The mean and the standard deviation are calculated using the following equations respectively:

$$\mu = \frac{1}{N}\sum_{i=1}^{N}\frac{O_i - B_i}{B_i} \tag{2.1}$$

$$\sigma = \sqrt{\frac{1}{N}\sum_{i=1}^{N}\left(\frac{O_i - B_i}{B_i} - \mu\right)^2} \tag{2.2}$$

where O_i is the observed value, B_i is the background value for the observation, i, in the model. The number of observations is denoted by N.

Innovations are calculated as the difference between the observations and background values for that particular observation, $O_i - B_i$. These are normalised through dividing the values by the NWP model background forecast which is represented by $\frac{O_i - B_i}{B_i}$. Normalised innovations for Metop-D are plotted against impact height (km) and are shown in Figure 2.1 and 2.2.

Metop-D's mean bias and standard deviation are somewhat comparable to those of the other Metop satellites, as seen in the top plot in Figure 2.1, with a more positive bias at heights $\geq$46 km and a maximum difference of 0.2% at 52 km. The standard deviation follows a similar trend throughout the atmospheric profile but is smaller at heights $\geq$26 km. The standard deviations are near-identical below 26 km, until 10 km where the standard deviation is again smaller for Metop-D.

A comparison between Metop-D, PlanetiQ and Spire in Figure 2.1 shows that the mean bias is similar between 6 and 49 km. Above 49 km, the biases for all three satellites begin to differ, but follow a similar pattern, with Metop-D exhibiting a more positive bias. Below 6 km, Metop-D is more negatively biased than PlanetiQ and Spire, with the largest difference of $\sim$0.7% and $\sim$1.0% between Metop-D, PlanetiQ and Spire, respectively. On the other hand, standard deviations have improved for Metop-D, being smaller overall. Between 10 and 15 km, the standard deviations are near-identical for all three satellites, while above 15 km, standard deviations for Metop-D are much smaller. Similarly, below 10 km, Metop-D has slightly smaller standard deviations than both comparison satellites.

It should be noted that PlanetiQ and Spire consist of constellations of satellites, whereas Metop-D is a single satellite. This is reflected in the number of occultations recorded over the same period,

with Metop-D, PlanetiQ and Spire having approximately 70,000, 435,000 and 125,000 occultations, respectively. During the calibration, validation and commissioning phase, instrument tests reduced the nominal sample size for Metop-D for this given period.

Figure 2.2 shows the BA bias for Metop-D comparing Met Office and ECMWF statistics. The mean bias is broadly consistent between the two NWP centres from 6 km to 40 km, with no dominant bias. Below 6 km, both the Met Office and ECMWF statistics exhibit increasingly negative biases, although the Met Office shows a slightly more negative bias in this region. Above ∼40 km, the mean bias diverges with the Met Office becoming positive while ECMWF exhibits a negative bias. The standard deviation again follows a similar trend between both centres; however, the Met Office has a smaller standard deviation than ECMWF above approximately 38 km.

Figure 2.3 shows the mean bias and standard deviation of Metop-D and Metop-C bending angles, separated by rising and setting occultations. For Metop-D, the mean biases of the rising and setting phases are similar throughout most of the profile in contrast to Metop-C, with small differences between the two phases above ∼49 km. Below 7 km, the mean bias for both Metop-D phases follow a similar behaviour, becoming increasingly negative with decreasing impact height. In contrast, Metop-C shows a stronger phase dependence at lower levels, with the setting phase remaining neutral whilst the rising phase becomes progressively more negatively biased. The standard deviations for rising and setting are broadly consistent throughout the atmospheric profile and similar for both Metop-D and C.

Figure 2.4 shows the mean bias and standard deviation of Metop-D and Metop-C bending angles, separated by latitude. The mean bias for both satellites is similar overall, with no major differences between them. Below 5 km, lower latitudes ($< 30^{\circ}$) exhibit a more negative bias for Metop-D than other latitudes at the same heights. Above 50 km, Metop-D shows a positive shift of ∼0.1% across all latitudes compared to Metop-C. The standard deviations are also similar between the two satellites, with Metop-D having smaller values observed for all latitudes above 37 km.

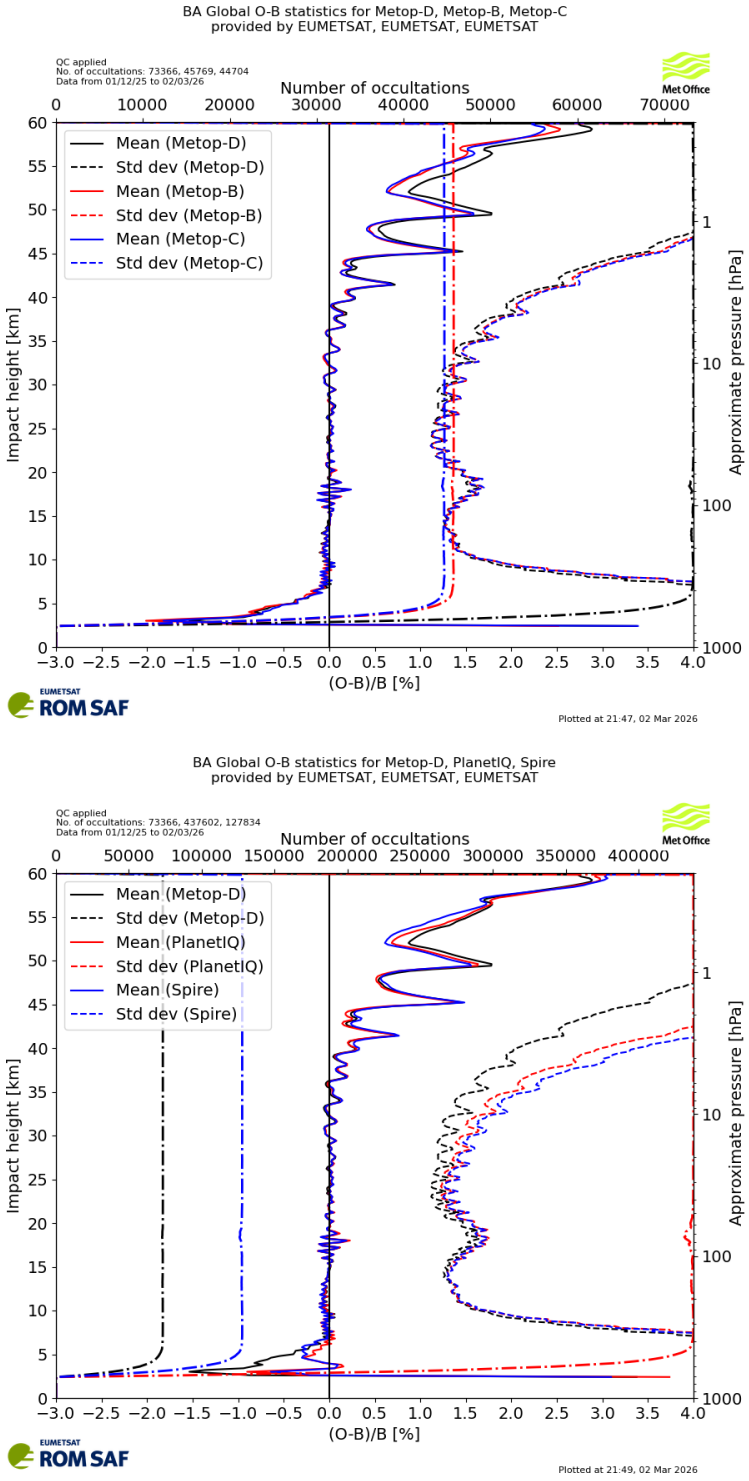

Figure 2.1: Seasonal plots of mean and standard deviations (where innovations are normalised by the model background, $(O-B)/B$) for Metop-D bending angles. Comparisons with Metop-B and Metop-C in the top plot and PlanetiQ and Spire in the bottom plot. Both are valid between 1st December 2025 and 2nd March 2026 and are all EUMETSAT-processed.

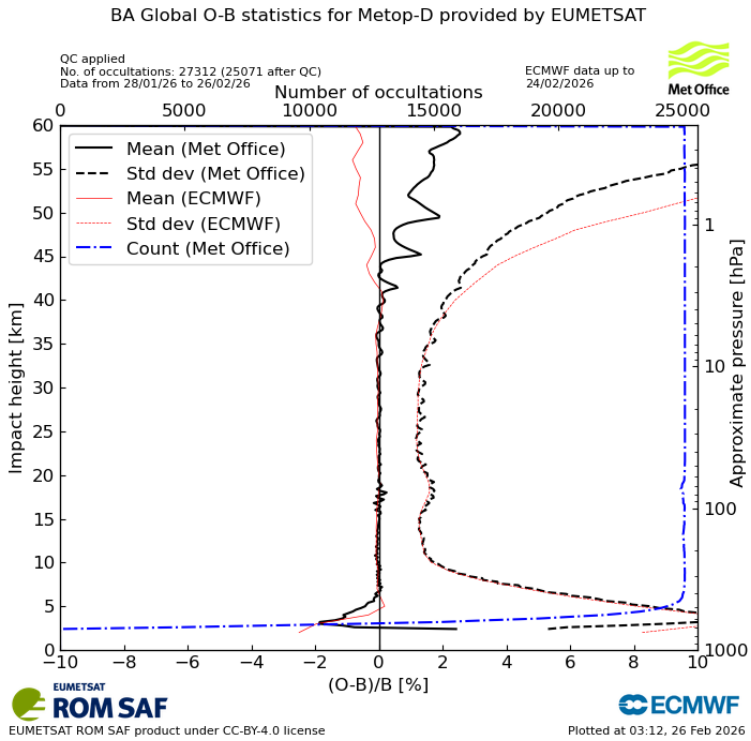

Figure 2.2: Monthly $O-B$ biases and standard deviations (where innovations are normalised by the model background, $(O-B)/B$) for Metop-D bending angles compared to ECMWF, for the period between 28th January 2026 and 26th February 2026.

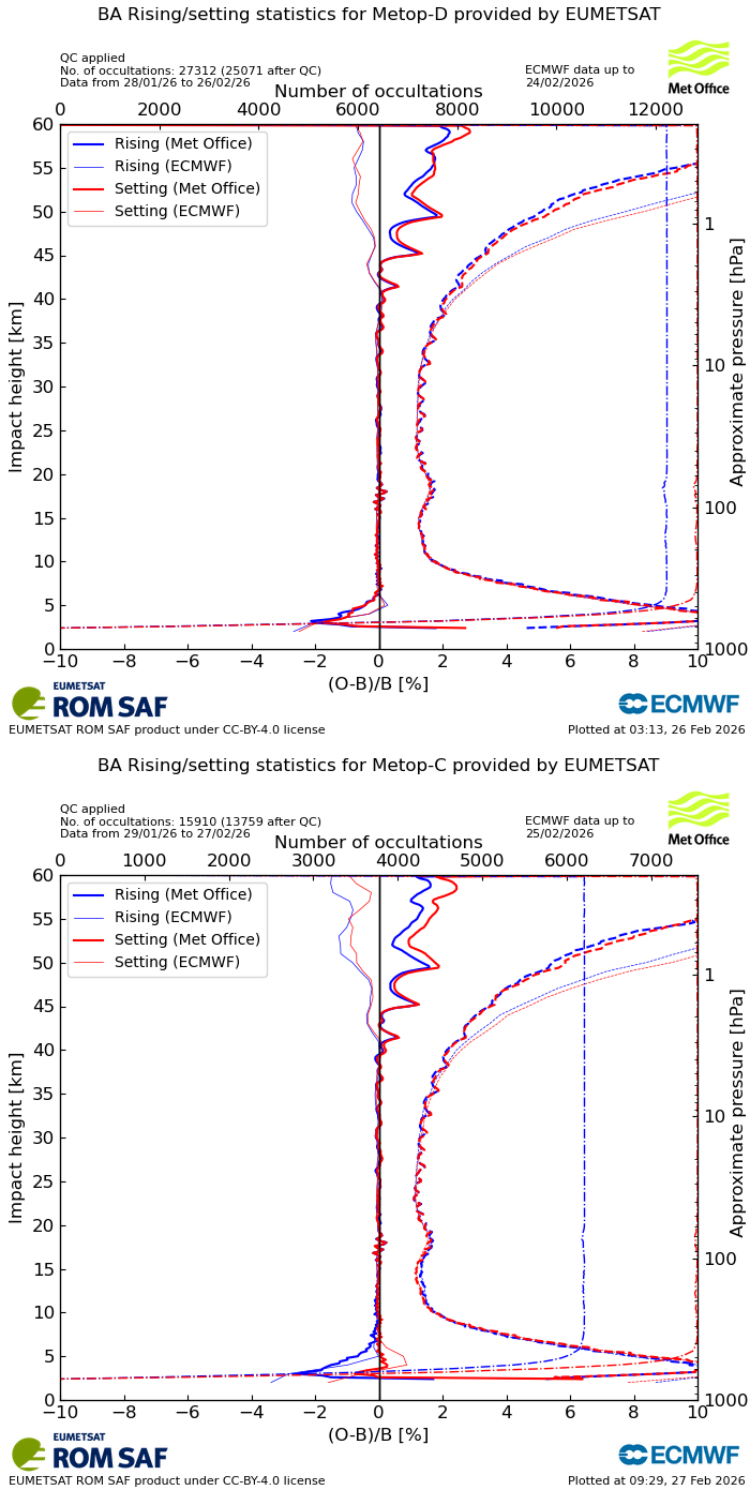

Figure 2.3: Monthly plots of mean and standard deviations (where innovations are normalised by the model background, $(O-B)/B$) for Metop-D (top) and Metop-C (bottom) separated by rising and setting phases, compared with ECMWF.

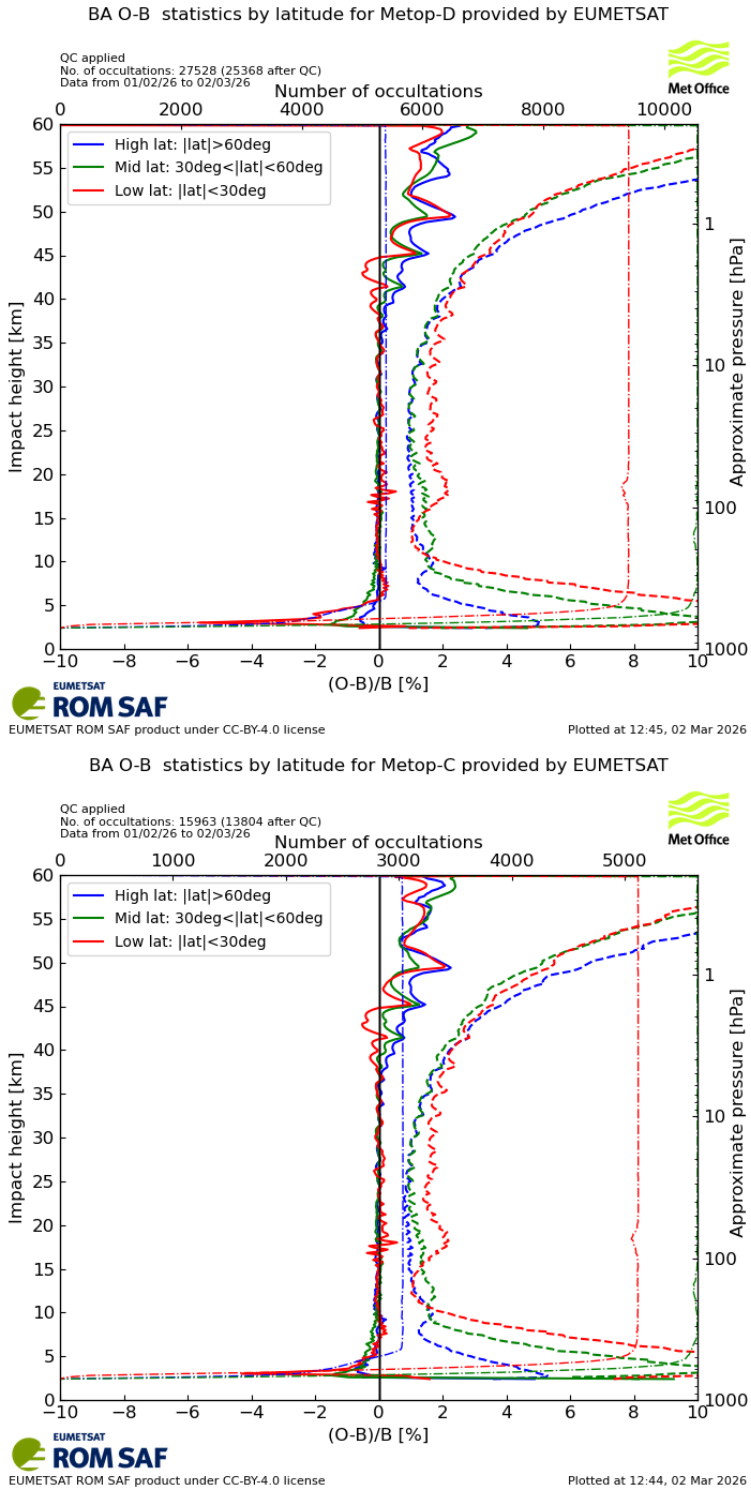

Figure 2.4: Monthly plots of mean and standard deviations (where innovations are normalised by the model background, $(O-B)/B$) for Metop-D (top) and Metop-C (bottom) separated by latitude.

2.2 Vertical correlations

Bending angle vertical correlations are important for NWP data assimilation as they provide information on the vertical structure of the atmosphere. We assume that the errors in the bending angle measurements are independent of each other (i.e. that the observation-error covariance matrix, $\mathbf{R}$, is diagonal). As this cannot be checked directly, the correlations in the innovation covariance matrix, $\mathbf{B}+\mathbf{R}$, can be calculated, and an attempt can be made to infer the behaviour of $\mathbf{R}$ from any features seen in the correlations. Due to the way bending angles are computed using the phase delay and Doppler shifts, positive correlations are expected close to the diagonal and negative correlations further away.

Figure 2.5 shows the vertical correlations for Metop-D, Metop-B, Metop-C and PlanetiQ. The structure of the vertical correlations are similar between all Metop satellites, showing near-diagonal correlation structure at all levels. PlanetiQ also exhibits a similar structure, although there are longe-range correlations which are not seen in the Metop satellite plots. As expected, there are positive correlations close to the diagonal and negative correlations further away. Above 43 km, negative correlations surrounding the diagonal are slightly broader in shape. In summary, the vertical correlation structure of Metop-D is consistent with other operational GNSS-RO satellites which meets the requirements for NWP data assimilation.

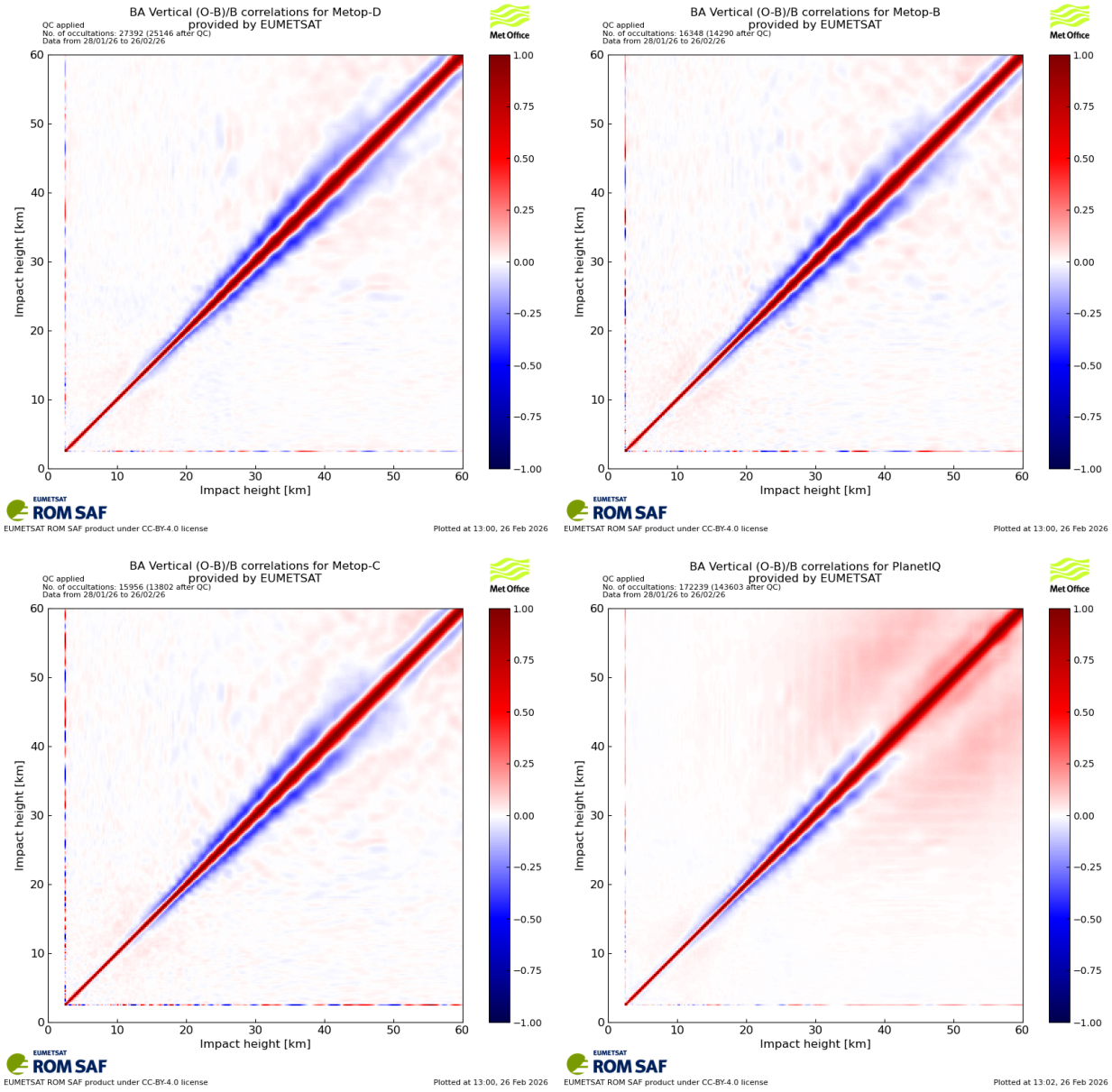

Figure 2.5: The vertical correlations for Metop-D (top-left), Metop-B (top-right), Metop-C (bottom-left), and PlanetiQ (bottom-right) bending angles. These are normalised differences between observations and background values from the NWP model.

3 Assimilation Experiments

This section details the assimilation experiments performed to assess the impact of Metop-D RO data on the Met Office's global forecasting system.

To evaluate the impact of Metop-D, an experiment was performed in which Metop-D observations were assimilated into the Met Office's NWP model. The results were compared against a corresponding control experiment covering the same period, which did not include Metop-D data. Both the trial and control experiments were run for three months, from 17th November 2025 to 17th February 2026. The first week was excluded from the verification statistics to allow time for the model to "spin up". Both experiments used a reduced-resolution, global, atmosphere-only configuration with a hybrid ensemble four-dimensional variational data assimilation system (hybrid 4D-Var). Both were run at N320 horizontal resolution giving 640×480 grid points, with 70 vertical levels. The control and trial produced forecasts every 12 hours, up to a lead time of 7 days.

The impact of assimilating Metop-D data is summarised using scorecards (see Figure 3.1). These scorecards show changes in forecast performance for different variables across the Northern Hemisphere extratropics (NH), Southern Hemisphere extratropics (SH) and Tropics (TR). The verification metric used is the root mean square error (RMSE), evaluated against observations and ECMWF analyses.

3.1 Scorecards

In these scorecards, green triangles indicate improvements to the forecast (a reduction in RMSE) relative to the control, while purple triangles indicate degradations (increase in RMSE) when adding Metop-D observations. Shaded squares denote statistical significance, and the area of each triangle represents the magnitude of the impact, with larger triangles indicating larger changes.

Figure 3.1 shows the verification against observations and ECMWF analyses. Verification against observations (left) shows an overall improvement of 0.19% in RMSE with positive impact seen. These improvements are distributed across NH and tropical regions for wind vectors, temperatures and geopotenial heights across the forecast ranges. Slight degradations are seen in the SH for temperature at 2 meters as well as geopotential height at 250 hPa and 500 hPa at shorter lead times.

The right scorecard in Figure 3.1 presents the scorecard for verification against ECMWF analyses which shows an overall impact of 0.20% in RMSE. Only minimal degradation for tropical temperature at 850 hPa and SH geopotential height at 500 hPa. Improvements are seen all aross the NH, as well as tropics for temperatures at 2 meters, 250 and 500 hPa. Positive impact is also observed in the SH for wind vectors and temperatures at 250 hPa.

After quality control, the Met Office assimilates approximately 14,000 observations per day. Metop-D is expected to contribute an additional 1,100 assimilated observations per day—a 7.9% increase—which is expected to contribute positively to forecast performance at the Met Office.

Figure 3.1: RMSE scorecards showing the impact of assimilating Metop-D data relative to the control, without Metop-D observations. This is for the period from 24th November 2025 to 17th February 2026. The left plot verified each trial against observations and the right plot verified against ECMWF analyses. $PMSL, W, T$ and Z represent the pressure at mean sea level, wind vectors, temperature and geopotential height respectively. NH, SH and TR are Northern Hemisphere extratropics, Southern Hemisphere extratropics and Tropics, respectively. The scorecards are also separated by vertical levels in each region – NH_T500 which represents temperature in the Northern Hemisphere extratropics at 500 hPa. The forecast lead times are shown in hours (i.e. $T+24$ is a 1-day forecast, $T+72$ is a 3-day forecast and so on). Green (purple) triangles indicate improvements (degradations); triangle area represents impact magnitude and shaded squares denotes statistical significance.

3.2 Other metrics

To fully understand the impact Metop-D has on the forecast system, other metrics are considered alongside the scorecards as these provide insight on individual components within the experiment.

Figure 3.2 shows the ratios of the standard deviation of the $O-B$ statistics for the experiment relative to the control. Negative (positive) ratio values indicate a reduction (increase) in standard deviation when Metop-D observations are assimilated into the NWP system. When adding RO observations, if there are improvements in the analyses and short-range forecast quality, then it is expected to also see an improvement in $O-B$ statistics for other observation types.

The results indicate that the addition of Metop-D data leads to a broadly neutral-to-beneficial impact on the forecast system. Considering the ratios for aircraft, surface and sondes variables (top panel of Figure 3.2), both aircraft and sonde observations show reduced standard deviations for relative humidity (RH), zonal and meridonal winds (U and V), and potential temperature (theta), indicating improved statistics of the assimilation. In contrast, surface observations show a small degradation, with relative humidity increasing by approximately $0.1 \pm 0.06\%$.

The bottom panel of Figure 3.2 shows the corresponding standard deviation ratios for satellite observations. As expected, the largest improvement is observed for GNSS-RO (GPSRO), with a reduction in standard deviation of approximately 0.45%. Smaller but consistent improvements are seen for several other instruments including Metop-B IASI (Infrared Atmospheric Sounding Interferometer) and Metop-C ATOVS (Advanced TIROS Operational Vertical Sounder). Additional reductions are evident for NOAA-20 ATMS and CrIS (Advanced Technology Microwave Sounder and Cross-track Infrared Sounder). The largest degradation is observed for AOD (aerosol optical depth) with an increase of around 0.1% which is consistent with the surface degradation seen in the top plot, since AOD gives the most benefit to 2-meter temperatures.

Aside from GNSS-RO, changes in $O-B$ standard deviations are generally small and mostly positive, indicating that the assimilation system for other instruments and observation types remain largely unaffected with no widespread degradation following the addition of Metop-D observations.

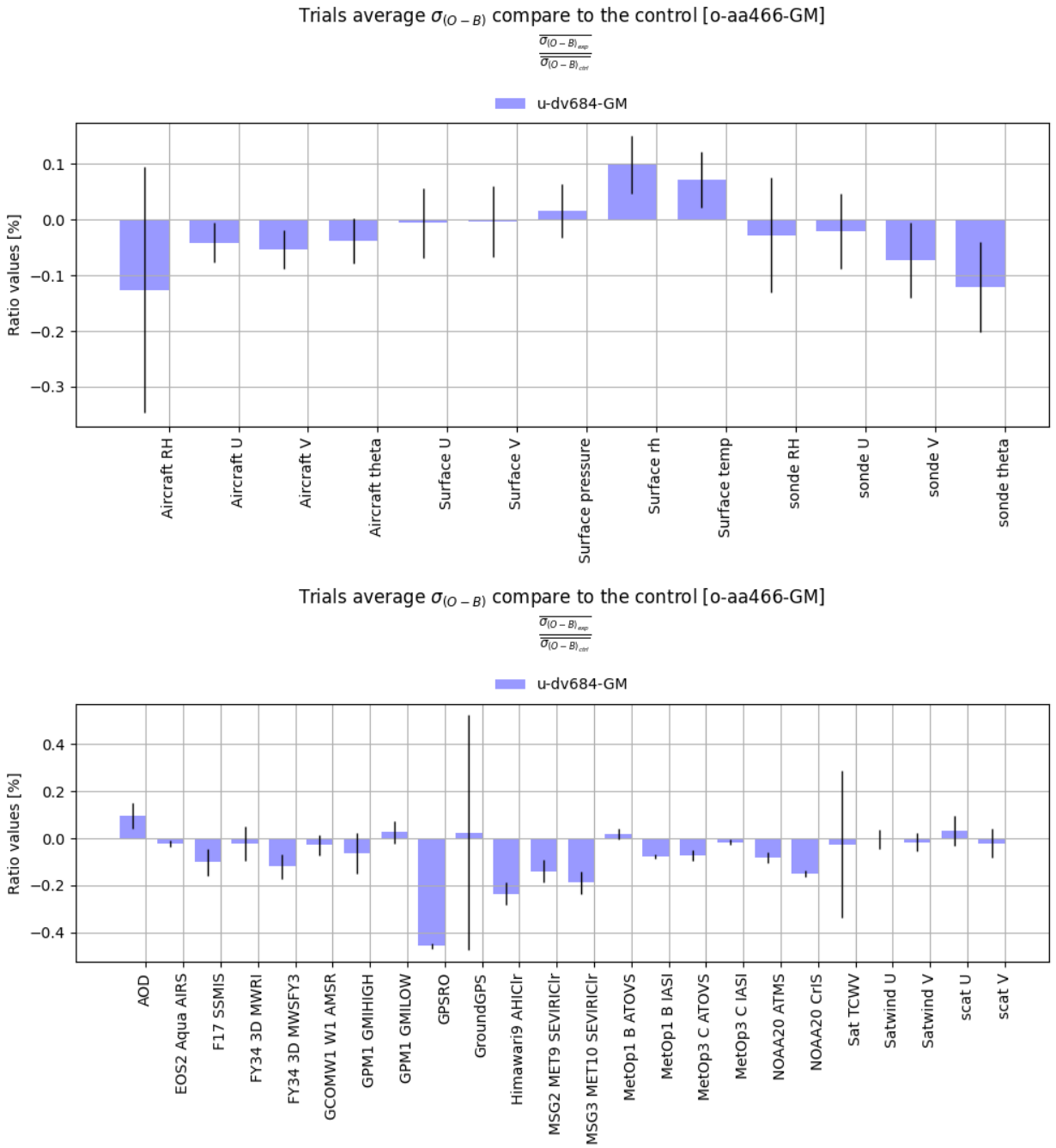

Figure 3.2: The two plots here show a summary comparing the experiment against the control without Metop-D data against other observations (top) and other satellites and instruments (bottom) for the period from 24th November 2025 to 17th February 2026.

4 Other Features

When monitoring satellite data, it is important to evaluate and assess other aspects of satellite data quality, such as timeliness, in addition to bending angles statistics.

4.1 Timeliness

Timeliness or delay is calculated at the time when the data is available in the Met Office's database from when the observations were made. Metop-D timeliness should be similar to Metop-B and Metop-C given that it is the first of EUMETSAT's second generation satellites. It was however, noted that during this monitoring period, Metop-D had an average delay of 1 hour and 45 minutes whereas Metop-B and Metop-C had an average delay of 52 minutes and 1 hour 20 minutes for the same period, respectively. Whilst the delay against other Metop satellites hasn't improved, it is however a significant improvement on FY-3E which had a delay of 3 hour 43 minutes (see Figure 4.1). Improvements are expected to be seen after the initial monitoring period when operational data transfer will be used.

In Figure 4.1, the green bars represent the observations that are received within three hours of the observation time, yellow bars represent observations received between three and six hours, and red bars represent observations received after six hours. At the Met Office, there are two runs for assimilating data: the *main* run assimilates data 2 hours and 40 minutes (the vertical dashed line) after the nominal time of the data assimilation window, while the *update* run assimilates observations approximately 6 hours after this window. Observations received after 6 hours are typically not assimilated in the global model.

Notably, 90% of the observations received from Metop-D are available from EUMETCast within 2 hours 06 minutes, which will be assimilated in the *main* run of the global model. This is a significant improvement compared to the initial FY-3E assessment, in which only around half of the observations were received before this time (Lewis, 2025). In Figure 4.1, 50% of FY-3E observations have only been received within 3 hours and 12 minutes so more than 50% are being cut off in for the *main* run.

4.2 Tandem flight

Metop-D is estimated to be assimilated in the Met Office NWP system around mid-2026, after the conclusion of a two-month tandem flight between Metop-C and Metop-D.

A tandem flight is a period during which two or more satellites are orbiting in close proximity to each other. During this time, Metop-D and Metop-C will be separated by approximately 30 seconds. Whilst this is useful for comparing and calibrating instruments on each satellite, it is not ideal for data assimilation in NWP models as near-duplicate observations can lead to overfitting of the analysis.

With a separation of ≈ 30 seconds, many occultations will sample similar atmospheric profiles for GPS but not BeiDou or Galileo, as Metop-C does not track these constellations. This leads to duplicated observations between Metop-C and Metop-D for GPS. The aim is to start operationally assimilating after the tandem period has completed to avoid the assimilation of redundant observations that do not provide additional benefit to the forecast skill and could lead to overfitting.

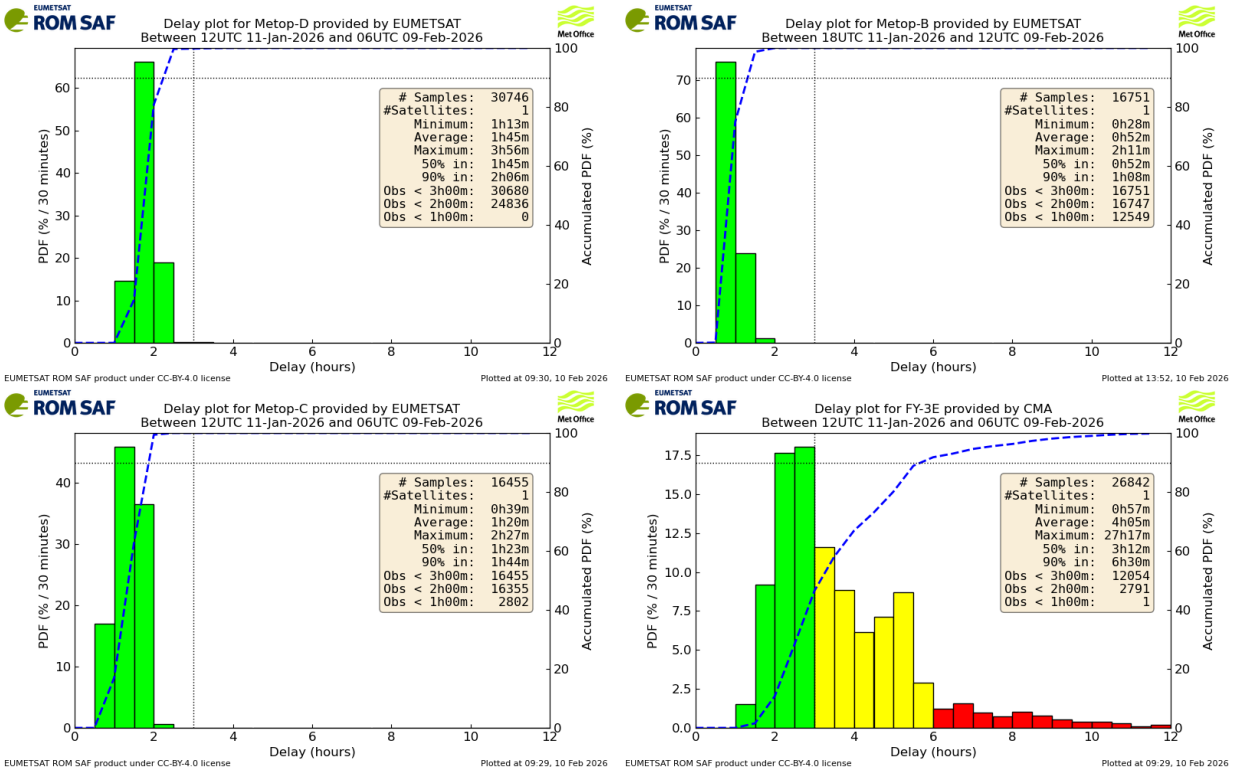

Figure 4.1: Delay histograms for Metop-D (top left), Metop-B (top right), Metop-C (bottom left) as well as FY-3E (bottom right). All datasets are processed by EUMETSAT, except FY-3E which is processed by the Chinese Meteorological Administration, CMA. The plots cover the period from 11th January 2026 to 9th February 2026.

5 Summary and Conclusions

Metop-D data have been available from EUMETCast for monitoring since 6th November 2025. Assimilation experiments demonstrate that the addition of around 1,100 RO profiles per day from Metop-D in the Met Office's NWP system has a clear positive impact on forecast performance.

Improvements of 0.19% and 0.20% in the root mean square error averaged over multiple variables is seen across both analyses, with most of the impact in the Northern Hemisphere extratropics and only minimal degradation in the Southern Hemisphere extratropics against observations.

The main points to highlight from the monitoring and evaluation are as follows:

- The mean bias and standard deviation of Metop-D are comparable to those of the other Metop satellites. The mean bias is more positive $\geq$ 46 km, while standard deviation is smaller below 10 km and above 25 km.
- Compared to Spire and PlanetiQ, Metop-D exhibits a more negative mean bias below 6 km, and a more positive mean bias between 49 and 57 km. The standard deviation follows a similar pattern but is smaller at all heights above 15 km, and slightly smaller below 10 km.
- Rising and setting statistics for Metop-D are similar to those for Metop-C, with divergence in mean bias observed above 39 km. Standard deviation is similar for both rising and setting phases, and is smaller when compared against ECMWF analyses.
- Bending angle statistics separated by latitude are largly similar with Metop-C, with minimal differences in mean bias and standard deviations.
- Vertical correlations for Metop-D are very similar to those of other GNSS-RO satellites, with only minimal variations above 43 km.
- Refractivity data are expected to become available from the end of March 2026 and will be assessed internally once disseminated.
- The addition of Metop-D primarily improves the consistency of RO assimilation, with a clear reduction of $O-B$ standard deviations, whilst maintaining a neutral-to-slightly positive impact on the wider observing system.
- The timeliness of Metop-D data is currently slower than that of other Metop satellites, but is expected to improve once operational data transfer is used.
- A tandem flight with Metop-C will conclude in the middle of 2026, after which Metop-D will be assimilated operationally within the Met Office.

Acknowledgments

With thanks to colleagues at the Met Office for their support in monitoring and help with the assimilation experiments of Metop-D data.

References

ESA (2026). *MetOp-SG instrument package*. https://www.esa.int/Applications/Observing_the_Earth/Meteorological_missions/MetOp_Second_Generation/MetOp-SG_instrument_package. Accessed: 2026-02-10.

Lewis, O. (2025). *An initial assessment of the quality of RO data from FY-3E*. ROM SAF Report SAF/ROM/METO/REP/RSR/047. Met Office. URL: https://rom-saf.eumetsat.int/general-documents/rsr/rsr_47.pdf.

ROM SAF (and earlier GRAS SAF) Reports

Reference	Report title
SAF/GRAS/METO/REP/GSR/001	Mono-dimensional thinning for GPS Radio Occulation
SAF/GRAS/METO/REP/GSR/002	Geodesy calculations in ROPP
SAF/GRAS/METO/REP/GSR/003	ROPP minimiser - minROPP
SAF/GRAS/METO/REP/GSR/004	Error function calculation in ROPP
SAF/GRAS/METO/REP/GSR/005	Refractivity calculations in ROPP
SAF/GRAS/METO/REP/GSR/006	Levenberg-Marquardt minimisation in ROPP
SAF/GRAS/METO/REP/GSR/007	Abel integral calculations in ROPP
SAF/GRAS/METO/REP/GSR/008	ROPP thinner algorithm
SAF/GRAS/METO/REP/GSR/009	Refractivity coefficients used in the assimilation of GPS radio occultation measurements
SAF/GRAS/METO/REP/GSR/010	Latitudinal Binning and Area-Weighted Averaging of Irregularly Distributed Radio Occultation Data
SAF/GRAS/METO/REP/GSR/011	ROPP 1dVar validation
SAF/GRAS/METO/REP/GSR/012	Assimilation of Global Positioning System Radio Occultation Data in the ECMWF ERA-Interim Re-analysis
SAF/GRAS/METO/REP/GSR/013	ROPP PP validation
SAF/ROM/METO/REP/RSR/014	A review of the geodesy calculations in ROPP
SAF/ROM/METO/REP/RSR/015	Improvements to the ROPP refractivity and bending angle operators
SAF/ROM/METO/REP/RSR/016	Simplifying EGM96 undulation calculations in ROPP
SAF/ROM/METO/REP/RSR/017	Simulation of L1 and L2 bending angles with a model ionosphere
SAF/ROM/METO/REP/RSR/018	Single Frequency Radio Occultation Retrievals: Impact on Numerical Weather Prediction
SAF/ROM/METO/REP/RSR/019	Implementation of the ROPP two-dimensional bending angle observation operator in an NWP system
SAF/ROM/METO/REP/RSR/020	Interpolation artefact in ECMWF monthly standard deviation plots
SAF/ROM/METO/REP/RSR/021	5th ROM SAF User Workshop on Applications of GPS radio occultation measurements
SAF/ROM/METO/REP/RSR/022	The use of the GPS radio occultation reflection flag for NWP applications
SAF/ROM/METO/REP/RSR/023	Assessment of a potential reflection flag product
SAF/ROM/METO/REP/RSR/024	The calculation of planetary boundary layer heights in ROPP
SAF/ROM/METO/REP/RSR/025	Survey on user requirements for potential ionospheric products from EPS-SG radio occultation measurements
SAF/ROM/METO/REP/RSR/026	Estimates of GNSS radio occultation bending angle and refractivity error statistics

continued on next page

continued

Reference	Report title
SAF/ROM/METO/REP/RSR/027	Recent forecast impact experiments with GPS radio occultation measurements
SAF/ROM/METO/REP/RSR/028	Description of wave optics modelling in ROPP-9 and suggested improvements for ROPP-9.1
SAF/ROM/METO/REP/RSR/029	Testing reprocessed GPS radio occultation datasets in a reanalysis system
SAF/ROM/METO/REP/RSR/030	A first look at the feasibility of assimilating single and dual frequency bending angles
SAF/ROM/METO/REP/RSR/031	Sensitivity of some RO measurements to the shape of the ionospheric electron density profile
SAF/ROM/METO/REP/RSR/032	An initial assessment of the quality of RO data from KOMPSAT-5
SAF/ROM/METO/REP/RSR/033	Some science changes in ROPP-9.1
SAF/ROM/METO/REP/RSR/034	An initial assessment of the quality of RO data from Metop-C
SAF/ROM/METO/REP/RSR/035	An initial assessment of the quality of RO data from FY-3D
SAF/ROM/METO/REP/RSR/036	An initial assessment of the quality of RO data from PAZ
SAF/ROM/METO/REP/RSR/037	6th ROM SAF User Workshop
SAF/ROM/METO/REP/RSR/038	An initial assessment of the quality of RO data from COSMIC-2
SAF/ROM/METO/REP/RSR/039	Impacts of RO mission differences on trends in multi-mission data records
SAF/ROM/METO/REP/RSR/040	Anomalous GRAS radio occultations
SAF/ROM/METO/REP/RSR/041	Assessment of sensitivity of the ROM SAF 1D-Var solutions to various error covariance choices
SAF/ROM/METO/REP/RSR/042	A one-dimensional variational ionospheric retrieval for truncated GNSS Radio Occultation measurements
SAF/ROM/METO/REP/RSR/043	Applying the ROPP ionospheric 1D-Var retrieval to Metop extension data
SAF/ROM/METO/REP/RSR/044	An investigation into the impacts of the vertical smoothing of GNSS-RO bending angle observations on Met Office NWP forecasts
SAF/ROM/METO/REP/RSR/045	TBA
SAF/ROM/METO/REP/RSR/046	8th EUMETSAT ROM SAF user workshop on GNSS radio occultation measurements
SAF/ROM/METO/REP/RSR/047	An initial assessment of the quality of RO data from FY-3E
SAF/ROM/METO/REP/RSR/048	TBA
SAF/ROM/METO/REP/RSR/049	An initial assessment of the quality of RO data from Metop-D

ROM SAF Reports are accessible via the ROM SAF website: https://rom-saf.eumetsat.int.